Available online at www.sciencedirect.com

ScienceDirect

Journal of Ocean Engineering and Science 5 (2020) 164–172

www.elsevier.com/locate/joes

Comparison of computational fluid dynamics and fluid structure interaction models for the performance prediction of tidal current turbines

Mujahid Badshah*, Saeed Badshah, Sakhi Jan

Department of Mechanical Engineering, International Islamic University, Islamabad, Pakistan

Received 24 June 2019; received in revised form 8 October 2019; accepted 8 October 2019
Available online 14 October 2019

Abstract

CFD models perform rigid body simulations and ignore the hydroelastic behavior of turbine blades. In reality, the tidal turbine blades deform due to the onset flow. Deformation of the turbine blade alters the angle of attack and pressure difference across the low pressure and high pressure surface of the blade. Therefore, the performance of a Tidal Current Turbine (TCT) is modelled in this study using Computational Fluid Dynamic (CFD) and coupled Fluid Structure Interaction (FSI) simulations to compare the predictions of both models. Results of the performance parameters predicted from both the models are also compared with experimental data. The difference between experimental value of C_P and predicted value from the rigid blade CFD and FSI models is less than 10%. The FSI model accounted for the blade deformation and a maximum blade tip deflection of 0.12 mm is observed representing a case of small deformation. The extent of deformation is not enough to alter the angle of attack and flow separation behavior at the blade. The variation in predicted pressure difference across the blade surfaces between the two models resulted in different C_P prediction. Almost similar wake predictions are obtained from both the models.

Keywords: Tidal turbine; Coupled FSI; CFD; Performance; ANSYS Wokbench; ANSYS CFX.

1. Introduction

Tidal current energy has the potential to provide a new renewable energy source to the world. Tidal energy technology has successfully gone through various development phases, with demonstration systems currently operating in relevant environments at pre-commercial and commercial scales [1,2]. Tidal Current Turbines (TCTs) often derive their design principals from wind turbine design [3]. However, there are certain key differences that needs careful consideration. These differences include that TCTs operate in different Reynolds Number R_e regimes, exhibit different stall characteristics and are subjected to harsh marine environment [4]. The proper understanding of device behavior is necessary to make this technology cost effective and reliable.

Numerical methods can be utilized to investigate the hydrodynamic performance of TCTs. Blade Element Momentum (BEM) is the most computationally efficient numerical method for computing the performance of TCTs, but it does not account for chord wise loading, variation in free stream flow and influence of rotor on the surrounding flow [5]. 3D inviscid methods like vortex lattice, lifting line and panel methods [6,7] can model the physics of turbine hydrodynamics in more detail than BEM method. However, these models do not account for the viscous effects that are essential for the accurate prediction of turbine performance. Computational Fluid Dynamics (CFD) models fluid flow by solving the Navier-Stokes equations and can capture viscous effects. Computational fluid dynamics (CFD) is the science of predicting fluid flow, heat and mass transfer, chemical reactions, and related phenomena by solving numerically the set of governing mathematical equations representing the conservation of mass, mo-

* Corresponding author.
E-mail address: mujahidbadshah@yahoo.com (M. Badshah).

https://doi.org/10.1016/j.joes.2019.10.001

Nomenclature

TSR	tip Speed Ratio
ω	blade Tip Angular Velocity, rad/s
R	turbine Radius, m
U_∞	mean upstream flow velocity, m/s
U	vector of velocity $U_{x,\ y,\ z}$, m/s
C_P	turbine Power Coefficient
C_T	turbine Thrust Coefficient
ρ	density of Water, Kg/m^3
AOA	angle of attack
Y^+	dimensionless wall distance
S_M	momentum source
τ	stress tensor
μ	dynamic viscosity

mentum, energy, species mass, etc. The fluid region is decomposed into a finite set of control volumes and the governing equations (continuous partial differential equations) are discretized into a system of linear algebraic equations that can be solved on a computer on this set of control volumes. A number of TCT turbine performance studies, based on CFD simulation, have been performed over the years. Tian et al. [8] used Reynolds Averaged Navier Stokes (RANS) CFD analysis to study the performance of a TCT. Their developed CFD method provided a good match with the experimental results for the power and thrust prediction of the TCT. Liu et al. [4] studied the effect of blade twist and nacelle shape on TCT performance. Shives and Crawford [9] performed CFD simulations to study the viscous loss, flow separation and base pressure effects in a duct augmented TCT. RANS CFD based numerical models have proved its capability to model the turbine hydrodynamics in more detail and with acceptable accuracy. However, the CFD models assumes the turbine blades to be rigid and ignores the hydroelastic interaction between the blades and flowing water. The rigid body assumption in the CFD models can have serious implications for the TCT performance assessment. A deflected turbine blade would present different angle of attack and pressure difference across the blade surfaces when compared to a rigid un-deflected blade. Most of the turbine CFD performance studies including those mentioned above have provided an acceptable accuracy compared to the experimental data because the turbine designs involved are of model scale and the blade deflections are minimal.

Numerical methods that can model interaction between the fluid and structure as well as taking into account the hydroelastic behavior of the structure called FSI methods can more closely assess the turbine performance. An FSI problem can be solved either through a monolithic or a partitioned approach. In the monolithic approach a single system of equation represents the structural mechanics and fluid dynamics systems that are solved simultaneously. In the partitioned approach the structure and fluid computational domains are treated separately and solved in their respective domains. Both the systems are represented by their respective systems of equations and are solved separately in their respective domains. A general classification of FSI methods applicable to all the related fields is very difficult. However, in the context of work presented in this paper the FSI methods can be classified into uncoupled, coupled and integrated approach. Interested readers may consult literature reported in [10–12] for more details. A loosely coupled modular approach is utilized in this paper, which is a partitioned/independent domain approach. The structural mechanics and fluid dynamics are solved in separate domains independent of each other. A coupling scheme is introduced to make the CFD and FEA codes communicate with each other. This approach has achieved great success in other related fields like marine propellers [13] but its use in the field of TCT is so far limited. Kim et al. [14] and Jo et al. [15] used the uncoupled FSI approach where the data transfer is executed after obtaining solution from a steady state CFD model with one way data transfer to investigate the structural integrity of turbine and tower respectively. Habib et al. [16] also used a similar post CFD mapping 1-way data transfer approach to model the vibration and fatigue response of TCT using FSI simulations. But this approach is only useful for modelling minimal nonlinearity. Nicholls-Lee et al. [17] although focused on the performance prediction and used a loosely coupled approach but a 2D panel code flow model is used. Suzuki and Mahfuz [18] also investigated the blade performance but their FSI model is based on an integrated approach by combining the beam element theory based structural solver and Blade Element Momentum Model for the hydrodynamics solver. Tatum et al. [19] performed the loosely coupled modular FSI simulations with two way data transfer. Similarly, we also used a loosely coupled modular independent domain FSI model with 2-way data transfer in our previous studies to model the structural mechanics and hydrodynamics of TCT [12,20]. But none of these studies provide an in depth analysis to establish the reason for difference in performance between a CFD model and FSI model representing a small deformation case. More such studies are required to further develop the understanding of these methods and suggest further improvements for the development of FSI models for the performance prediction of TCT.

In this paper coupled FSI simulations with two way data transfer are performed to model the performance of a horizontal axis TCT. The ANSYS system coupling is used to couple the CFD solver ANSYS CFX with structural solver ANSYS transient structural in the ANSYS Workbench to setup a transient coupled FSI simulation. Performance of the turbine is simulated at the optimum TSR with uncoupled rigid body transient CFD and coupled transient FSI simulations. Performance of the turbine predicted with both the numerical models is compared with the experimental data [21]. The paper is structured into 4 sections. Section 2 presents the numerical method with mesh setup in Section 2.1 and model setup in Section 2.2. Results are discussed in Section 3 and the conclusions are outlined in Section 4.

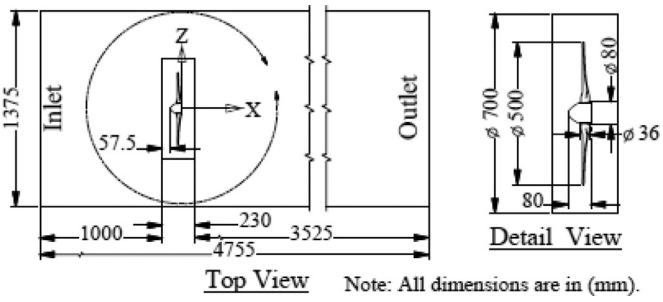

Fig. 1. Geometric details of turbine and computational domain.

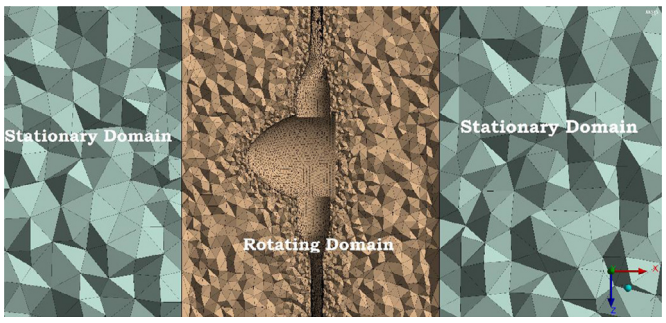

Fig. 2. CFD Mesh.

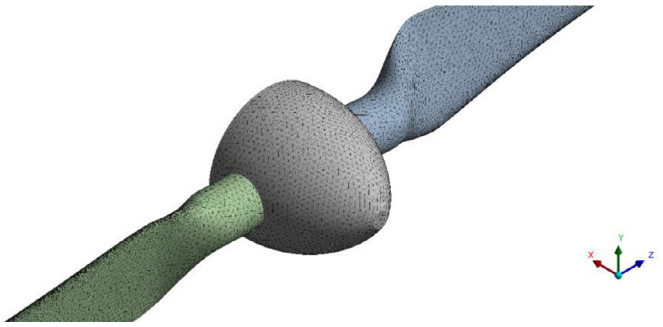

Fig. 3. FEA Mesh.

2. Numerical method

CFD simulations are performed with the node centered finite volume solver Ansys CFX within the Ansys workbench. The fluid region is meshed to be decomposed into finite number of control volumes. The general conservation (transport) equation for continuity and momentum given below are solved on the set of control volume:

$$\frac{\partial \rho}{\partial t} + \nabla.[\rho U] = 0 \tag{1}$$

$$\frac{\partial [\rho U]}{\partial t} + \nabla.[\rho U \otimes U] = -\nabla \rho + \nabla.\tau + S_M \tag{2}$$

The stress tensor,τ, is related to the strain rate by:

$$\tau = \mu\left[\nabla U + [\nabla U]^T - \frac{2}{3}\,\delta \nabla.U\right] \tag{3}$$

The turbine design utilized in this study is a 1:40 scale model of the RM1 turbine design [21]. RM1 is originally a counter rotating twin rotor turbine each having a rotor diameter of 0.5 m. Only one rotor is used for the study in this paper due to symmetry of the design. For the simulations performed in this study, two fluid domains are defined (Fig. 1).

The external domain is of rectangular shape [1.375 × 1 × 4.755 m]. The width of domain [1.375 m] is half the width of the experimental channel because only one rotor of the twin rotor turbine is modelled. The depth of the domain [1 m] is equal to the flow depth of the experimental channel. The length [4.75 m] of the domain is set such that it was equivalent to 10 rotor diameters (10D), a length suggested to be enough for obtaining a solution not effected by the end conditions [22,23]. Additionally, we have verified in one of our previous studies [24] that the length of domain (10D) is sufficient to obtain a performance estimate unaffected by the pressure outlet condition for the utilized turbine design and flow conditions. Rotor of the turbine is enclosed in a cylindrical domain of 0.70 m diameter to rotate it about an axis. The length of this domain is 0.23 m and it was located at 1 m from the inlet. Two simulations, a URANS CFD and a coupled FSI simulation, are conducted at the optimum operating condition corresponding to a TSR 5.11. This TSR is selected because it represents the peak power condition [21] and the largest bending moments will occur at this TSR [25]. One of the simulation represented the turbine as a rigid structure and utilized the uncoupled URANSCFD model. While the other simulation was setup as a coupled FSI model. In this model the CFD and Finite Element Model are coupled using the system coupling system of the Ansys workbench. This model has the capability to account for the blade deformation in response to the hydrodynamic forces acting on the blades.

2.1. Mesh setup

Two separate meshes are generated as the CFD and FEA mesh for this study as shown in Figs. 2 and 3.

The CFD mesh with 3.98 million tetrahedral elements is generated at the rectangular stationary and cylindrical rotating domains. The turbine domain had 1.92 million elements with inflation layers around blade surfaces to accurately model the flow separation and reattachment. This mesh setup provides a mesh independent CFD solution. A mesh sensitivity study has not been exclusively performed for the presented study. However, we have provided a detailed mesh independence study for a similar CFD model in our previous study [24]. The FEA mesh utilized the rotor geometry as a solid with 0.89 million solid 187 elements.

2.2. Model setup

For the CFD system the Unsteady Reynold Averaged Navier Stokes (URANS) equations are solved with a transient rotor stator approach. A sliding mesh technique is utilized to physically rotate the turbine domain. Shear Stress Transport (SST) turbulence model is used with an automatic wall

Table 1
CFD Model Parameters.

Parameter	Setting
Analysis Type	Multifield coupling-None, Total time-0.6 s, Timestep-0.0016 s
Cylindrical Domain	Non Buoyant, Rotating, Turbulence- SST, Wall function-Automatic
Rotor	No Slip Wall, Rotating at 21.48 rad/s, Mesh Motion option-unspecified/System Coupling, Mesh deformation- regions of motion specified
Inlet	Subsonic, Normal speed-1.05 m/s, Medium Turbulence Intensity 5%
Outlet	Subsonic, static pressure-0Pa
Side wall	Symmetry
Bottom and other side	No slip wall
Top	Free slip wall
Three Interfaces	General connection, Transient rotor stator, Mesh connection-GGI
Convergence criteria	RMS residual $1\times E^{-4}$

function approach. The SST turbulence model can accurately predict the onset and amount of flow separation in adverse pressure gradients [26]. The SST model has demonstrated better flow separation prediction and more accurate performance assessment in several turbine CFD studies [27,28]. The wall function model utilizes the log law approximation and provides better computational efficiency. Summary of the CFD model parameters is outlined in Table 1.

The bottom and one side wall of the computational domain are assigned "no slip wall" conditions. Walls are solid (impermeable) boundaries to fluid flow. No slip walls are the most common type of wall boundary condition implementation. For no slip walls the fluid immediately next to the wall assumes the velocity of the wall, which is zero by default. This boundary condition was the most appropriate to represent the physical model of experimental water channel in this study since these experiments were conducted in a flow tank and not a towing tank. For the coupled FSI simulation, mesh deformation is activated for the rotating domain with specified regions of motions having displacement relative to previous mesh and the mesh motion settings of rotor are changed to receive mesh motion from system coupling.

The FEA system (i.e., Transient structural system in ANSYS Workbench) utilized solid blades with structural steel material for the simplicity of the FEA model. This simplification was required to lower the model complexity at the initial model development phase. The use of steel blades will not affect the findings of this study and its relevance to real turbine blades made from composite materials. Because this study is focused on the comparison of CFD and FSI models for the performance prediction of TCT. The overall behavior of variation in performance and load characteristics will remain same irrespective of the blade material. The use of steel instead of composite material will only change the amount of blade deformation which is not the focus of this study. The material properties of the utilized structural steel material for turbine blades are as in Table 2.

Table 2
Properties of the utilized structural steel material for turbine blades.

Density	7850	Kg/m^3
Young Modulus	2E+11	Pa
Poisson's Ratio	0.3	(-)
Tensile Yield Strength	2.5E+08	Pa
Compressive Yield Strength	2.5E+08	Pa
Tensile Ultimate Strength	4.60E+08	Pa

A remote displacement support is applied to the rear face of the hub. Remote displacement is a type of constraint that enables to apply rotation at an arbitrary location in space. A rotational velocity of 21.48 rad/s corresponding to the optimum turbine TSR of 5.1 is assigned to the rotor to account for the effect of centrifugal forces in the FEA system. A fluid solid interface boundary condition is applied on all faces comprising the rotor blades. The ANSYS Workbench platform is then used to couple the FEA and CFD analysis system through system coupling component system. Total simulation time of 0.6 s with a time step of 0.0016 s is set for the system coupling to make the time settings similar to the two participating component systems. This time setting corresponds to two rotations of the turbine with a time step of 2° rotation. Two data transfers are setup to transfer force data from CFD to FEA system and incremental displacement from the FEA system as mesh displacement to the CFD system. The contributing regions for the data transfer is the fluid solid interface boundary setup at the blade surfaces in the FEA system and no slip wall boundary comprising of blade surfaces in CFD. Execution sequence for the simulation is setup such that 1st the FEA system is solved. In general terms this is a loosely coupled modular FSI arrangement. Where the system coupling acted as a black box that receive data from each participating system and then transfer it to the other system in an iterative manner at each coupling step. Flow chart of the FSI solution procedure is shown in Fig. 4.

The CFD simulation was considered to be converged when the difference of predicted torque values between consecutive iterations became negligible. Fig. 5 shows a screen shot of the convergence plot of turbine torque from the CFD solver participating in the coupled FSI simulation. It is clearly evident from Fig. 5 that the torque value will change minimally with further iterations and the solution is converged. A similar convergence plot was obtained from the RANSCFD simulation but is not provided here for brevity. Another important convergence parameter for the coupled FSI simulation is the convergence of data transfer values, which is the fluid force on the blades in this case. Fig. 6 clearly shows that RMS change in data transfer values for the simulation presented in this paper has also converged.

3. Results and discussion

To discuss results in this paper, the following non dimensional performance parameters are used:

$$\text{Tip Speed Ratio}: \quad TSR = \omega R/U_\infty \tag{4}$$

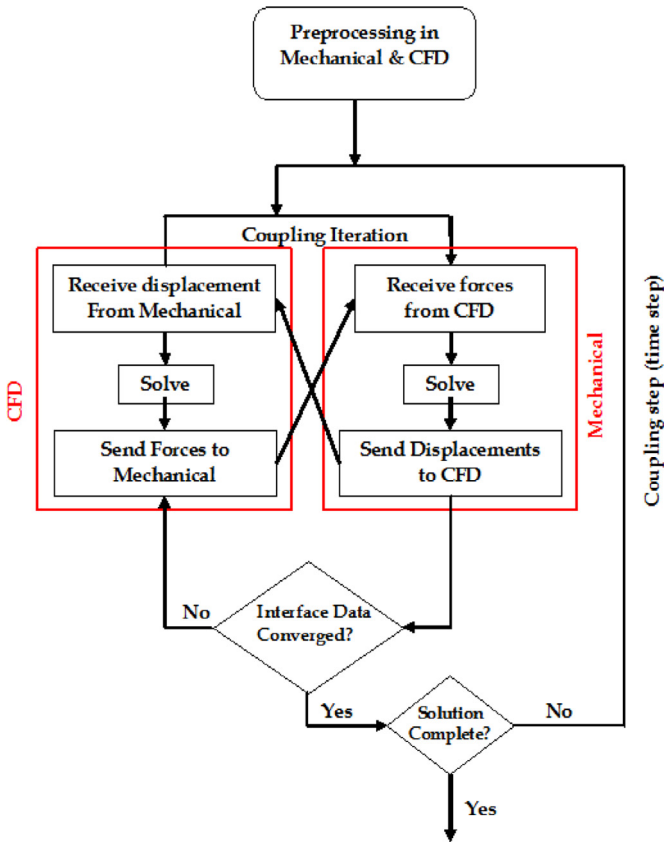

Fig. 4. Loosely coupled modular FSI solution procedure.

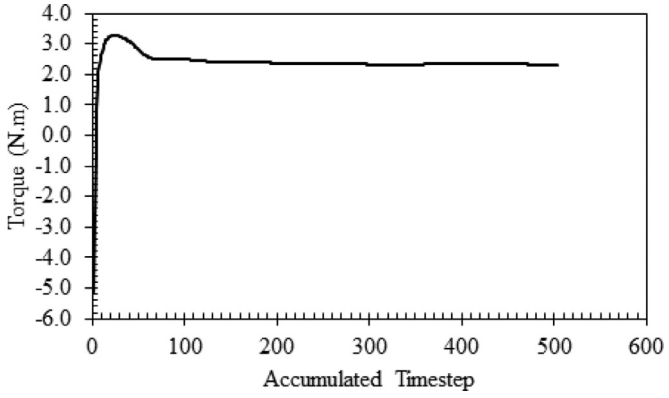

Fig. 5. Convergence plot of turbine torque from the CFD solver participating in coupled FSI simulation.

$$\text{Power Coefficient}: \; C_P = P/0.5\rho A U_\infty^3 \tag{5}$$

$$\text{Thrust Coefficient}: \; C_T = T/0.5\rho A U_\infty^2 \tag{6}$$

In these equations U_∞ (m/s) represent the free stream velocity, ω (rad/s) the angular speed of the blade tip (assumed constant for the simulations conducted in this paper), R (m) the radius of the rotor, A (m^2) the swept area of the rotor, P (watts) the total power available in the flow stream and T (N) is the force acting along the flow direction.

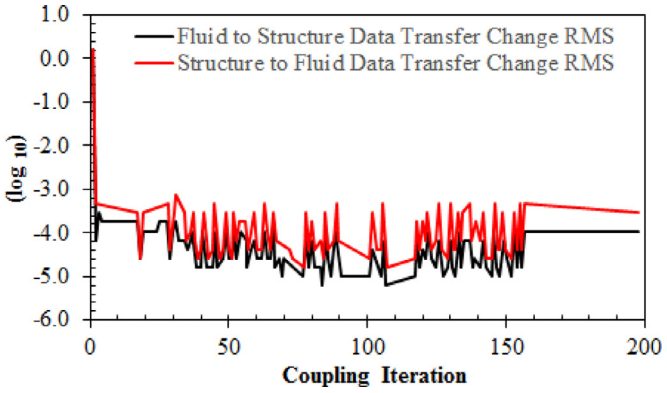

Fig. 6. Convergence plot of data transfers from the coupled FSI simulation.

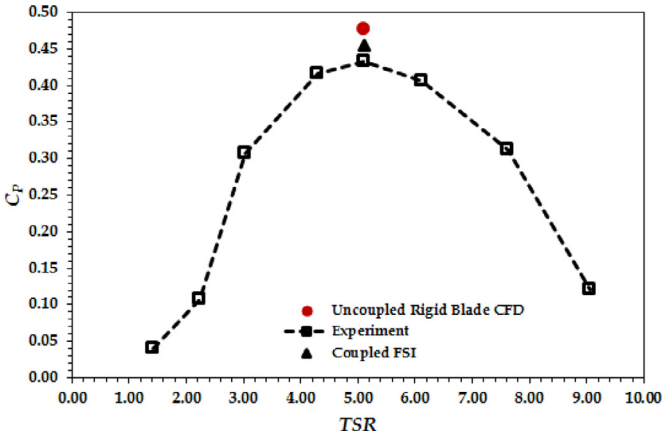

Fig. 7. Comparison of experimental and simulated performance coefficient.

Table 3
Quantitative comparison of Numerical and Experimental predictions.

	Torque (N.m)	C_P (-)	Thrust (N)	C_P Error (%)
Experiment	2.08	0.4337	–	–
Uncoupled CFD Model	2.28	0.4761	100.22	9.78
Coupled FSI Model	2.18	0.4545	99.29	4.80

To compare the accuracy of the utilized modelling techniques the simulated results are plotted against the experimental data [21]. Fig. 7 shows the comparison of power coefficient C_P obtained from the CFD simulations and experiments.

The quantitative comparison of experimental data and predictions of the numerical models are as in Table 3.

The difference between experimental value of C_P and predicted value from the rigid blade CFD and FSI models was less than 10%. The coupled FSI model predicted a lower value of turbine C_P(0.45) compared to a C_P value of 0.48 predicted by the uncoupled rigid blade CFD model. This is in contrast to Tatum et al. [19] where the FSI model predicted a greater value of C_P than the uncoupled CFD model. Tatum et al. [19] attributed this discrepancy to the fact that initially blades of their turbine were not in its optimum position. A thrust force of 100.22 N and 99.29 N is predicted by the uncoupled CFD and FSI models respectively.

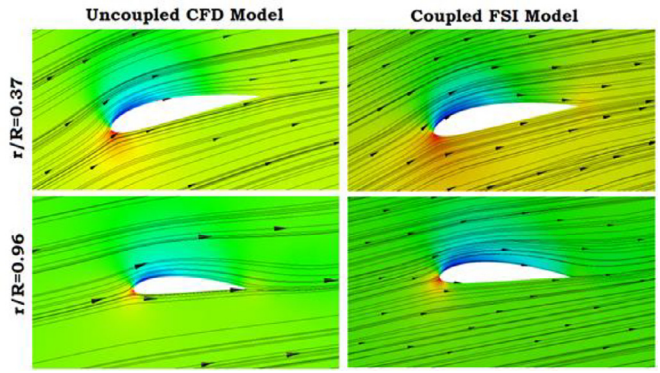

Fig. 8. Pressure contour with velocity streamlines at TSR 5.11.

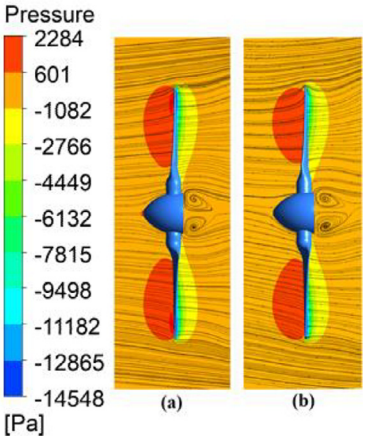

Fig. 9. Pressure contour with velocity streamlines at the blade tip (a) Uncoupled CFD (b) Coupled FSI.

Experimental data for the thrust force is not available to validate the thrust results and evaluate the prediction error. However, the prediction pattern is totally in accordance to the physical observation that the deformed blade will experience a lesser thrust as compared to an undeformed blade. To further investigate the reason for the difference in C_P prediction between the two numerical models, pressure contour with velocity stream lines at blade sections at 37% and 96% of the blade length are plotted in Fig. 8.

Both the numerical models clearly show fully attached flow at both the blade sections. The blade deformation has not resulted in a significant change in the angle of attack that could have resulted in any variation in the separation and reattachment behaviour. However, the pressure contour shows a difference in pressure at low pressure side of the blade for both models. To more clearly elaborate this difference, pressure contour along the blade length with velocity streams is plotted in Fig. 9.

The maximum pressure for the uncoupled CFD model is more as compared to the coupled FSI model. To further visualize changes in the flow behavior due to blade deformation, velocity contour at 96% of the blade length for both models is plotted in Fig. 10.

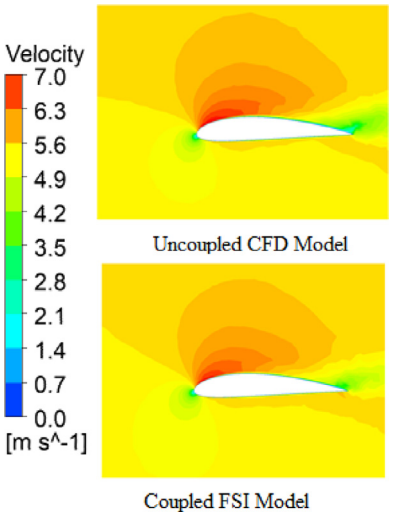

Fig. 10. Velocity contour around foil at the blade tip.

A small increase in local flow velocity along the high pressure side of the foil encircled in red can be clearly observed for the coupled FSI model. Reading Fig. 5 along with Figs. 6 and 7, the reason for the difference in C_P prediction between the two models is attributed to the difference in pressure difference and flow velocity across the low pressure and high pressure side of the blade. In the coupled FSI model the blade has deflected but the extent of deflection is not enough (0.12 mm) to create a significant variation in the angle of attack but it certainly has changed the pressure difference and flow velocity across the blade surfaces. The pressure difference across the blade surfaces is responsible for generating the lift force. For the uncoupled CFD model the pressure difference is more therefore, the predicted C_P is on higher side.

One of the advantage of a loosely coupled modular FSI approach is that results of individual component systems can be post processed in their respective post processors. All the results that are possible in standalone FEA and CFD system solutions can be obtained in a similar way. Although structural investigations are not the scope of this paper, however, the deformation and equivalent stress on rotor is provided in Fig. 11 to exactly know their extent.

Fig. 12 shows the time histories of deformation and stress predicted by the FSI model at every time step during the solution. A maximum deformation of 0.116 mm occurred at the blade tip. This deformation is very small due to reasons that the blade is completely solid and made from structural steel. It is highly unlikely for a real turbine blade to be made in this manner but this simplification is necessary to reduce the modelling complications at this stage of the model development.

To further compare the performance of the two models, the centerline velocity deficit prediction of the two models is plotted against the experimental data in Fig. 13. The figure clearly shows that the wake prediction of both the models upto 6D downstream is almost similar. This may be due to the fact that the maximum deformation of the blade is only

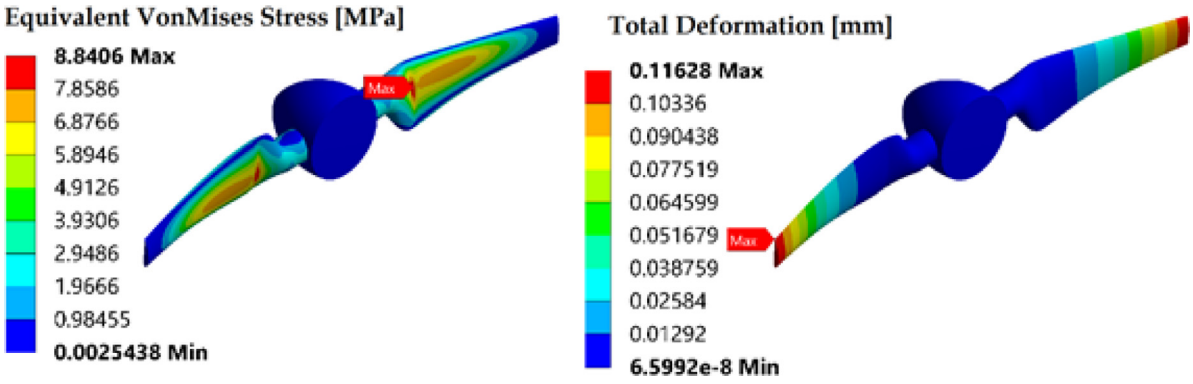

Fig. 11. Stress and deformation contour at the rotor.

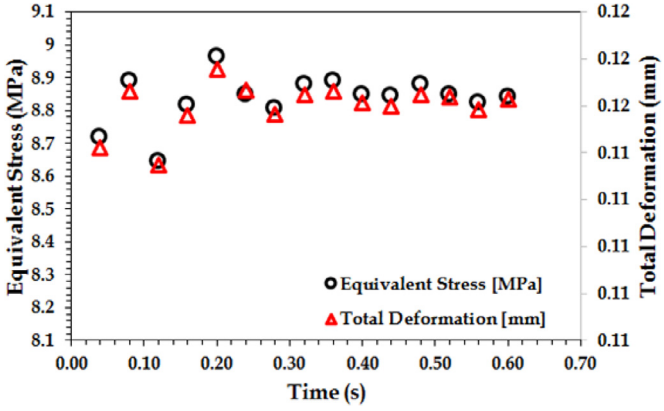

Fig. 12. Stress and deformation at the rotor at every time step during the FSI solution process.

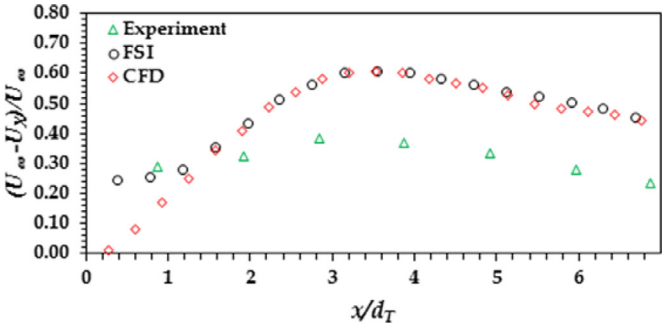

Fig. 13. Comparison of rotor hub height velocity deficit prediction.

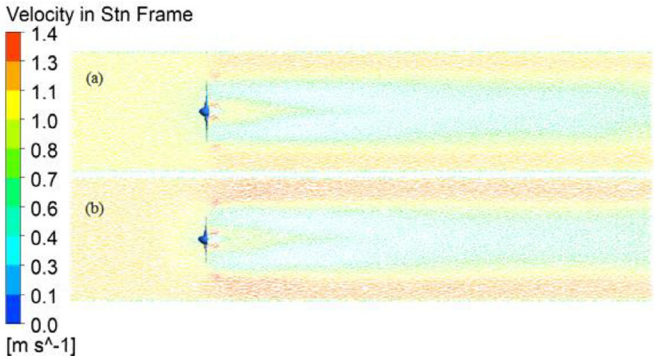

Fig. 14. Velocity vectors plotted on a vertical plan along the rotor center line (a) Uncoupled CFD model (b) Coupled FSI Model.

0.12 mm which is not expected to make a huge difference in the wake prediction. The other important aspect of the wake results is that the prediction of both models does not conform to the experimental data. This could be due to the effect of cross arms, tower and left side rotor. These effects are not included in the numerical model for simplicity. Additionally, the simulations presented in this paper utilized CFD based on Reynolds Averaged Navier Stokes (RANS) models. In this approach the time averaged Navier–Stokes equation are solved through turbulence model to solve all the turbulent length scales. An SST turbulence model belonging to the group of eddy viscosity model based on the Boussinesq hypothesis is used. The Boussinesq hypothesis is based on the assumption of isotropic turbulence, which is only valid for small scale turbulence. On the contrary, turbulence in the wake region of a TCT is strongly anisotropic in nature [29] and the size of turbulence structure is of the same order of magnitude as the diameter of turbine [30]. The accurate modelling of downstream wake would require Large Eddy Simulations (LES) models that solves the spatially averaged Navier-Stokes equations and directly resolve large turbulence structures. Furthermore, the experimental wake data is upto 25D whereas the simulated wake data is upto 7D. To obtain a clear comparison between the experimental and numerical velocity deficit data, a farther velocity deficit plot from the numerical model will be required. Since far wake study is not the objective of this work, therefore, a shorter domain length of 10D is used to achieve a better computational efficiency. To gain an insight of the flow passing through the turbine, the stationary frame velocity vectors are plotted along a vertical plane passing through the centerline of the rotor (see Fig. 14). Almost a similar flow behavior has been captured by both models.

Although both the numerical models predict the turbine performance and wake with almost similar accuracy but the requirement of computational resource and solution time are very different. Both the uncoupled CFD and coupled FSI simulations presented in this paper are performed on the HP Z840 Workstation with Intel(R) Xeon(R) CPU E5-2699 v3

Table 4
Details of computational resource and time.

Numerical Model		No. of Utilized Cores	Solution Time		
			Days	Hours	Minute
Uncoupled- CFD	Steady State RANS	30 Cores/60 Partitions	–	2	30
	Transient RANS	36 Cores/72 Partitions	–	3	9
Coupled- FSI	Transient RANS	18 Cores/36 Partitions	11	19	16
	FEA	04 Cores and 1 GPU			

@ 2.30 GHz, 36 Core(s), 72 Logical Processor(s) having an Installed Physical Memory (RAM) of 128 GB. The details of utilized computational resource and time is as in Table 4.

Although, the computational resources dedicated to different simulations are not similar. However, Table 4 still provides a clear picture of the computational solution time requirement for both the methods. The uncoupled CFD model clearly has far lower solution time compared to the coupled FSI model.

The CFD and FSI modelling approaches have their distinct features and use. Both these techniques have their unique positions as research tools in the modern day research and may never be considered as a replacement of one another. However, for the tidal turbine performance modelling, the CFD model is less complicated, computationally efficient and require less computational resources. Whereas, the FSI models are capable to model the turbine structural response that could be crucial for the turbine performance estimates in the case of large blade deformation.

4. Conclusion

Uncoupled transient URANS CFD and coupled FSI simulations of the RM1 TCT design are performed to numerically model its performance. Results from both numerical models are compared with experimental data of RM1 model turbine. The turbine performance results predicted by both the rigid blade CFD and coupled FSI model matched well with the experimental data. The difference between experimental value of C_P and predicted value from the rigid blade CFD and FSI models was less than 10%. There is not much to choose between the two models on the basis of turbine C_P prediction for the evaluated cases. The coupled FSI model predicted a lower value of turbine C_P(0.45) compared to a C_P value of 0.48 predicted by the uncoupled rigid blade CFD model. The difference in prediction of both the numerical models is very small. Because, the experiment and numerical model both utilized a small scale model with solid blades representing a small deformation case. For more realistic cases involving larger blade deformation, the difference between the prediction of rigid blade CFD and FSI model is expected to considerably increase. Therefore, it is concluded that for cases involving larger blade deformation, the FSI models will be more adequate to obtain an accurate representation of the turbine performance. The FSI model accounted for the blade deformation and a maximum blade tip deflection of 0.12 mm is observed. The extent of deformation was not enough to alter the angle of attack and flow separation behavior at the blade. The variation in predicted pressure difference across the blade surfaces between the two models resulted in different C_P prediction. Two-way coupled FSI has been shown that it can be a powerful tool in understanding the critical points in a device design. Coupled FSI model can identify potential failure points and areas of over design. A similar wake behavior is predicted by both the models because the turbine blade tip deflection was not significant for the simulated turbine design. The computational expense of the coupled FSI model is much higher than the uncoupled RANS CFD model. Therefore, it is concluded that they may only be preferred for turbine performance prediction cases involving larger blade deformations or when the focus of investigation is to determine the structural response in terms of stresses, deformation or fatigue evaluation.

Declaration of Competing Interest

The authors declare that they have no known competing financial interests or personal relationships that could have appeared to influence the work reported in this paper.

Acknowledgments

The authors gratefully acknowledge the support of the Department of Aeronautics and Astronautics at the Institute of Space Technology (IST) Islamabad for providing computational facilities at the modelling and simulation laboratory.

References

[1] M. Davide, U. Andreas. 2014 JRC ocean energy status report. EUR 26983 EN. Publications Office of the European Union, Luxembourg, 2015. p. 15. https://doi.org/10.2790/866387.
[2] S.P. Neill, A. Vogler, A.J. Goward Brown, S. Baston, M.J. Lewis, P.A. Gillibrand, et al., Renew. Energ. 114 (2017) 3–17.
[3] M.J. Khan, G. Bhuyan, M.T. Iqbal, J.E. Quaicoe, Appl. Energ. 86 (2009) 1823–1835, doi:10.1016/j.apenergy.2009.02.017.
[4] J. Liu, H. Lin, S.R. Purimitla, M.D. ET, Appl. Ocean Res. 64 (2017) 58–69.
[5] I. Masters, J. Chapman, M. Willis, J. Orme, J. Marine Eng. Technol. 10 (2011) 25–35.
[6] P. Liu, Energy 35 (2010) 2843–2851.
[7] S.A. Kinnas, W. Xu, Y.H. Yu, L. He, J. Offshore Mech. Arctic Eng. 134 (2012) 011101.
[8] W. Tian, J.H. VanZwieten, P. Pyakurel, Y. Li, Energy 111 (2016) 104–116, doi:10.1016/j.energy.2016.05.012.
[9] M. Shives, C. Crawford, Proc IMechE, Part A: J Power and Energy 226 (2012) 112–125.

[10] R.F. Nicholls-Lee, S.R. Turnock, S.W. Boyd, in: Proceedings of the 7th International Conference on Computer and IT Applications in the Maritime Industries (COMPIT'08), 2008, pp. 314–328.
[11] G. Hou, J. Wang, A. Layton, Commun. Comput. Phys. 12 (2012) 337–377.
[12] M. Badshah, S. Badshah, K. Kadir, Energies 11 (2018) 1–13.
[13] S. Turnock, A. Wright, Mar. Struct. 13 (2000) 53–72, doi:10.1016/S0951-8339(00)00009-5.
[14] B. Kim, S. Bae, W. Kim, S. Lee, M. Kim, in: IOP Conf. Series: Earth and Environmental Science, 2012, doi:10.1088/1755-1315/15/4/042037042037.
[15] C.-.H. Jo, D.-.Y. Kim, Y.-.H. Rho, K.-.H. Lee, C. Johnstone, Renew. Energy 54 (2013) 248–252.
[16] U. Habib, M. Hussain, N. Abbas, H. Ahmad, M. Amer, M. Noman, J. Ocean Eng. Sci. (2019).
[17] R. Nicholls-Lee, S. Turnock, S. Boyd, Renew. Energy 50 (2013) 541–550.
[18] T. Suzuki, H. Mahfuz, Ships Off Shore Struct. 13 (2018) 451–458.
[19] S.C. Tatum, C.H. Frost, M. Allmark, D.M. O'Doherty, A. Mason-Jones, P.W. Prickett, et al., Int. J. Mar. Energy 14 (2016) 161–179, doi:10.1016/j.ijome.2015.09.002.
[20] M. Badshah, S. Badshah, J. VanZwieten, S. Jan, M. Amir, S.A. Malik, Energies 12 (2019) 2217.
[21] H. Craig, S.N. Vincent, G. Budi, G. Michele, S. Fotis, U.S. Department of Energy Reference Model Program RM1: Experimental Results. Technical Report; 2014. Available online: https://www.osti.gov/biblio/1172793-department-energy-reference-model-program-rm1-experimental-results, doi:10.2172/1172793, (accessed on 19th October 2019).
[22] H.J. Chul, Y.Y. Jin, H.L. Kang, H.R. Yu, Renew. Energ. 42 (2011) 195–206, doi:10.1016/j.renene.2011.08.017.
[23] K. Nitin, B. Arindam, Appl. Energ. 148 (2015) 121–133, doi:10.1016/j.apenergy.2015.03.052.
[24] M. Badshah, J. VanZwieten, S. Badshah, S. Jan, IET Renew. Power Gen. (2019), doi:10.1049/iet-rpg.2018.5134.
[25] P. Ouro, M. Harrold, T. Stoesser, P. Bromley, J. Fluids Struct. 71 (2017) 78–95.
[26] ANSYS Inc., ANSYS CFX-Solver Modelling Guide, ANSYS Inc., Canonsburg, PA, USA, 2016, p. 146.
[27] S.F. Sufian, M. Li, B.A. O'Connor, Renew. Energ. 114 (2017) 308–322, doi:10.1016/j.renene.2017.04.030.
[28] A. Elhanafi, J. Ocean Eng. Sci. 1 (2016) 268–283.
[29] S. Tedds, I. Owen, R. Poole, Renew. Energ. 63 (2014) 222–235.
[30] I.A. Milne, R.N. Sharma, R.G. Flay, S. Bickerton, Philos. Trans. R. Soc. A 371 (2013) 20120196.